

Dark and multi-dark solitons in the three-component nonlinear Schrödinger equations on the general nonzero background

Zhi-Jin Xiong(熊志进)[1], Qing Xu(许庆)[2], Liming Ling(凌黎明)[2]
Citation: Chin. Phys. B . 2019, 28(12): 120201 . **doi:** 10.1088/1674-1056/ab50fc
Journal homepage: http://cpb.iphy.ac.cn; http://iopscience.iop.org/cpb

What follows is a list of articles you may be interested in

Resonant multiple wave solutions to some integrable soliton equations

Jian-Gen Liu(刘建根)[1,2], Xiao-Jun Yang(杨小军)[1,2,3], Yi-Ying Feng(冯忆颖)[2,3]
Chin. Phys. B . 2019, 28(11): 110202 . **doi:** 10.1088/1674-1056/ab4d47

Exact solutions of a (2+1)-dimensional extended shallow water wave equation

Feng Yuan(袁丰), Jing-Song He(贺劲松), Yi Cheng(程艺)
Chin. Phys. B . 2019, 28(10): 100202 . **doi:** 10.1088/1674-1056/ab3e65

Dynamics of three nonisospectral nonlinear Schrödinger equations

Abdselam Silem, Cheng Zhang(张成), Da-Jun Zhang(张大军)
Chin. Phys. B . 2019, 28(2): 020202 . **doi:** 10.1088/1674-1056/28/2/020202

A note on “Lattice soliton equation hierarchy and associated properties”

Xi-Xiang Xu(徐西祥), Min Guo(郭敏)
Chin. Phys. B . 2019, 28(1): 010202 . **doi:** 10.1088/1674-1056/28/1/010202

N-soliton solutions for the nonlocal two-wave interaction system via the Riemann-Hilbert method

Si-Qi Xu(徐思齐), Xian-Guo Geng(耿献国)
Chin. Phys. B . 2018, 27(12): 120202 . **doi:** 10.1088/1674-1056/27/12/120202

Dark and multi-dark solitons in the three-component nonlinear Schrödinger equations on the general nonzero background*

Zhi-Jin Xiong(熊志进)[1], Qing Xu(许庆)[2], and Liming Ling(凌黎明)[2,†]

[1] School of Electric Power Engineering, South China University of Technology, Guangzhou 510640, China
[2] School of Mathematics, South China University of Technology, Guangzhou 510640, China

(Received 29 August 2019; revised manuscript received 9 October 2019; published online 15 November 2019)

We exhibit some new dark soliton phenomena on the general nonzero background for a defocusing three-component nonlinear Schrödinger equation. As the plane wave background undergoes unitary transformation $SU(3)$, we obtain the general nonzero background and study its modulational instability by the linear stability analysis. On the basis of this background, we study the dynamics of one-dark soliton and two-dark-soliton phenomena, which are different from the dark solitons studied before. Furthermore, we use the numerical method for checking the stability of the one-dark-soliton solution. These results further enrich the content in nonlinear Schrödinger systems, and require more in-depth studies in the future.

Keywords: dark soliton, three-component nonlinear Schrödinger equations, general nonzero background

PACS: 02.30.Ik, 03.75.Lm, 42.81.Dp **DOI:** 10.1088/1674-1056/ab50fc

1. Introduction

Research of multi-component nonlinear Schrödinger (MCNLS) equations has attracted a great deal of attention since they can be used to describe a variety of complex physical phenomena (Bose–Einstein condensates,[1] nonlinear optics,[2] superfluid,[3] and alpha helical protein,[4] etc.), and they possess more abundant dynamical patterns of localized wave solutions (soliton,[5] rogue wave[6–8]) than ones in scalar models. Particularly, soliton is an important nonlinear phenomenon in nonlinear Schrödinger systems. Various solitons and other defects have been experimentally observed and theoretically investigated, such as dark soliton,[9] bright soliton,[10] vector soliton,[11–13] kink,[14] and magnon,[15] etc. Among these solitons, dark soliton has been found to appear in defocusing nonlinear systems arising in nonlinear optics[16] and Bose–Einstein condensates,[17] etc.

For research of soliton on the integrable nonlinear Schrödinger system, most of the previous studies focus on the zero background or non-vanishing background.[18–22] Meanwhile, there are lots of results for the soliton solutions on the nonlinear Schrödinger-typed models with variable coefficient or high dimension.[23–29] More than a decade ago, Shin found dark soliton solutions on a cnoidal wave background in a defocusing medium.[30] Recently, Lan *et al.* presented different profiles of dark-solitons on stripe phase background in a two-component Bose–Einstein condensate.[31] Motivated by the above-mentioned two works, it is natural to ask whether there exist some dark solitons on the general nonzero background for the nonlinear Schrödinger system.

To the best of our knowledge, there is almost no work on discussing the dark soliton for the three-component nonlinear Schrödinger (TCNLS) equations on the general nonzero background. In this work, we study dynamics of the single dark soliton and two dark solitons for the TCNLS equations on the general nonzero background, and obtain various general nonzero backgrounds by adjusting parameters. Furthermore, the collision of two dark solitons also shows the elastic interaction between solitons on the general nonzero background. These new phenomena enrich the study of the dark solitons on various backgrounds and provide the theoretical basis for physical experiment.

This paper is organized as follows. In Section 2, we give the $SU(3)$ transformation for the TCNLS equations and study the modulational instability of the general nonzero background solution by the linear stability analysis. In Section 3, we study the propagation of single-dark soliton and discuss the collision between the two dark solitons on the general nonzero background. Then we test the numerical stability of the single dark soliton on the general nonzero background by numerical method. Section 4 involves some discussions and conclusions.

2. General nonzero background solution and its modulational instability analysis

In this section, we mainly study the general nonzero background solutions and modulational instability for the TCNLS

*Project supported by the National Natural Science Foundation of China (Grant No. 11771151), the Guangdong Natural Science Foundation of China (Grant No. 2017A030313008), the Guangzhou Science and Technology Program of China (Grant No. 201904010362), and the Fundamental Research Funds for the Central Universities of China (Grant No. 2019MS110).

†Corresponding author. E-mail: linglm@scut.edu.cn

© 2019 Chinese Physical Society and IOP Publishing Ltd

equations

$$\mathrm{i}\boldsymbol{q}_t+\frac{1}{2}\boldsymbol{q}_{xx}-\boldsymbol{q}\boldsymbol{q}^{\dagger}\boldsymbol{q}=0, \tag{1}$$

where $\boldsymbol{q}=(q_1,q_2,q_3)^{\mathrm{T}}$ with q_1, q_2, q_3 being the functions with respect to space x and time t, the symbols † and T denote the conjugate transpose and transpose, respectively. The TCNLS equations (1) possess the $SU(3)$ symmetry. In other words, the solutions to the TCNLS equations are invariant under the $SU(3)$ transformation, i.e. if $\boldsymbol{q}$ is a solution to the TCNLS equations (1), so does $\boldsymbol{A}\boldsymbol{q}$, here $\boldsymbol{A}\in SU(3)$, i.e. the matrix $\boldsymbol{A}$ satisfies $\boldsymbol{A}\boldsymbol{A}^{\dagger}=\mathbb{I}$, $\mathbb{I}$ is the identity matrix, then we will obtain some solutions possessing the novel dynamic behavior. It is easy to observe that the plane wave solution

$$q_i=c_i\mathrm{e}^{\mathrm{i}\theta_i},\ \ \theta_i=a_ix-\left(\frac{a_i^2}{2}+c_1^2+c_2^2+c_3^2\right)t,\ \ i=1,2,3, \tag{2}$$

satisfies the TCNLS equations (1). Combining the $SU(3)$ transformation and the plane wave solution (2), we can obtain the general nonzero background solution, which is constituting of three different periodic functions. In the following, we study the general nonzero background solution deeply. Here we should stress that general nonzero background solution is different from the algebraic geometry solution by algebraic curve with high genus.[32]

2.1. General nonzero background

In this subsection, we discuss the general nonzero background solutions, which are totally different from the original plane wave solutions. The general nonzero background solutions can be written as

$$\begin{aligned} q_k &= A_{k1}c_1\mathrm{e}^{\mathrm{i}(a_1x-g_1t)}+A_{k2}c_2\mathrm{e}^{\mathrm{i}(a_2x-g_2t)}+A_{k3}c_3\mathrm{e}^{\mathrm{i}(a_3x-g_3t)},\\ k &= 1,2,3, \end{aligned} \tag{3}$$

where $g_i=\frac{a_i^2}{2}+\sum_{l=1}^{3}c_l^2$, $i=1,2,3$, a_1, a_2, and a_3 jointly determine the characteristics of general nonzero background, and the amplitude of the wave background is decided by c_1, c_2 and c_3, the matrix $\boldsymbol{A}=(A_{i,j})_{1\leq i,j\leq 3}$ is an element of unitary group $SU(3)$. We can notice that the new solution possesses the periodic or non-periodic behavior, which depends on the specific values of a_k and g_k $(1\leq k\leq 3)$. For the two-component case, the background will turn to the periodic background since there are two different phase factors under the $SU(2)$ transformation.[31]

In what follows, we would like to analyze the dynamics for general nonzero background solution in detail. Based on the zero elements in the matrix $\boldsymbol{A}$, we classify them into three cases as follows.

Case 1 If we choose $\boldsymbol{A}$ as the identity matrix

$$\boldsymbol{A}=\begin{bmatrix}1&0&0\\0&1&0\\0&0&1\end{bmatrix},\quad \boldsymbol{q}=\begin{bmatrix}c_1\mathrm{e}^{\mathrm{i}(a_1x-g_1t)}\\c_2\mathrm{e}^{\mathrm{i}(a_2x-g_2t)}\\c_3\mathrm{e}^{\mathrm{i}(a_3x-g_3t)}\end{bmatrix}, \tag{4}$$

then the solution is just the original seed solution. Its modulus is constant, it is easy to study it. Most of the previous studies about dark soliton were in this background, so here we do not discuss it.

Case 2 If we consider another special form, which is analogous to the two-component condition, i.e. $\boldsymbol{A}\in SU(1)\oplus SU(2)$, it can be expressed as

$$\boldsymbol{A}=\begin{bmatrix}0&1&0\\\frac{\sqrt{2}}{2}&0&\frac{\sqrt{2}}{2}\\-\frac{\sqrt{2}}{2}&0&\frac{\sqrt{2}}{2}\end{bmatrix},\ \boldsymbol{q}=\begin{bmatrix}c_2\mathrm{e}^{\mathrm{i}(a_2x-g_2t)}\\\frac{\sqrt{2}}{2}c_1\mathrm{e}^{\mathrm{i}(a_1x-g_1t)}+\frac{\sqrt{2}}{2}c_3\mathrm{e}^{\mathrm{i}(a_3x-g_3t)}\\-\frac{\sqrt{2}}{2}c_1\mathrm{e}^{\mathrm{i}(a_1x-g_1t)}+\frac{\sqrt{2}}{2}c_3\mathrm{e}^{\mathrm{i}(a_3x-g_3t)}\end{bmatrix}. \tag{5}$$

This case has been discussed in the previous work,[31] so here we ignore it.

Case 3 In the following, we mainly discuss the general situation, where matrix $\boldsymbol{A}$ has all nonzero elements. Then we calculate the intensity of background $|q_1|^2$, $|q_2|^2$, and $|q_3|^2$, which are written as

$$\begin{aligned} |q_i|^2 =& \sum_{m=1}^{3}A_{im}^2c_m^2+\sum_{n=1,l=1,n<l}^{3}2A_{in}A_{il}c_nc_l\\ &\times\cos\left[(a_n-a_l)\left(x-\frac{a_n+a_l}{2}t\right)\right], \end{aligned} \tag{6}$$

where A_{im} $(i,m=1,2,3)$ are the elements of the corresponding row and column in matrix $\boldsymbol{A}$, and the utmost amplitude of the three backgrounds is $\sum_{n=1,l=1,n<l}^{3}2A_{in}A_{il}c_nc_l$, $(i=1,2,3)$.

From the expression of Eqs. (6), we can realize that the magnitude of fluctuation of general nonzero background is determined by three cosine functions, and the amplitude of fluctuation is approximately along three families of straight lines:

$$\begin{aligned} &(a_n-a_l)\left(x-\frac{1}{2}(a_n+a_l)t\right)=k_j\pi,\\ &n,j,l=1,2,3,\ n<l, \end{aligned} \tag{7}$$

where k_1,k_2,k_3 are integral numbers. The magnitude of fluctuation can be maximized, and the parameters k_1,k_2,k_3 must satisfy the relationship

$$k_2=k_1+k_3. \tag{8}$$

In the following, we discuss the influence on the fluctuation of general nonzero background by the parameters. By analyzing the expressions, we can obtain that the variation with time and space is determined only by the parameters a_1, a_2, a_3. According to the their values, we can divide the situation into three categories.

Case I For $a_1=a_2=a_3$, the amplitude of background will be constant and the background will also become a plane wave background.

Case II For $a_1=a_2$, $a_3\neq a_2$, the fluctuation of background will be decided by one cosine function, which will form the periodic background, the situation has been studied in the literature.[31]

Case Ⅲ While a_1, a_2, a_3 are not equal to each other, this general situation is too complicated to analyze completely. However, we will roughly divide the case into four categories in the next section.

Based on the special setting of parameter matrix $\boldsymbol{A}$, we can obtain different dynamics of background solutions with the aid of numeric method. We will exploit the dark solitons on the general nonzero background and observe its dynamic behavior in the following section, which provides a new researchable background for dark soliton experiments on diverse physical fields.

2.2. Modulational instability analysis

In this subsection, we study the modulational instability (MI) for the general nonzero background solution through the linear stability analysis. Considering the complexity of matrix $\boldsymbol{A}$, we choose the case that matrix $\boldsymbol{A}$ equals to the unit matrix $\mathbb{I}$ to study the MI. The other cases can be studied in a similar procedure. Then adding the perturbation into background solutions (2), we can obtain

$$q_j = (c_j + \varepsilon u_j)\mathrm{e}^{\mathrm{i}(a_j x - g_j t)},\ (j = 1,2,3), \tag{9}$$

where ε is a very small parameter, and u_1, u_2, u_3 are the functions with respect to x and t. Substituting Eq. (9) into the TC-NLS Eq. (1), and ignoring the higher terms $(\varepsilon^2, \varepsilon^3)$ and keeping the ε^0 and ε^1 terms, then we can obtain the equations

$$\begin{aligned}
&\mathrm{i}u_{1,t} + \mathrm{i}a_1 u_{1,x} + \frac{1}{2}u_{1,xx} - (c_1c_3(u_3^* + u_3) \\
&\quad + c_1c_2(u_2^* + u_2) + c_1^2(u_1^* + u_1)) = 0, \\
&\mathrm{i}u_{2,t} + \mathrm{i}a_2 u_{2,x} + \frac{1}{2}u_{2,xx} - (c_2c_3(u_3^* + u_3) \\
&\quad + c_1c_2(u_1^* + u_1) + c_2^2(u_2^* + u_2)) = 0, \\
&\mathrm{i}u_{3,t} + \mathrm{i}a_3 u_{3,x} + \frac{1}{2}u_{3,xx} - (c_3c_2(u_2^* + u_2) \\
&\quad + c_3c_1(u_1^* + u_1) + c_3^2(u_3^* + u_3)) = 0.
\end{aligned} \tag{10}$$

Then we can assume the solutions of u_j $(j = 1,2,3)$ as the Fourier modes

$$u_j = u_{j,1}\mathrm{e}^{\mathrm{i}kx} + u_{j,2}\mathrm{e}^{-\mathrm{i}kx},\ j = 1,2,3, \tag{11}$$

where $u_{j,1}$ and $u_{j,2}$ are the periodic functions only about t, and k is the wave number. Then substituting Eq. (11) into Eq. (10), we can obtain a series of equations rewritten as the matrix form

$$\boldsymbol{U}_t = \boldsymbol{H}\boldsymbol{U}, \tag{12}$$

where $\boldsymbol{U} = (u_{11}, u_{12}^*, u_{21}, u_{22}^*, u_{31}, u_{32}^*)^{\mathrm{T}}$, and the coefficient matrix $\boldsymbol{H}$ is

$$\begin{aligned}
\boldsymbol{H} &= \mathrm{i}\left(\boldsymbol{\Phi} - k\boldsymbol{\Psi} + \frac{k^2}{2}\boldsymbol{\Theta}\right),\ \boldsymbol{\Psi} = \mathrm{diag}(a_1, a_1, a_2, a_2, a_3, a_3), \\
\boldsymbol{\Theta} &= \mathrm{diag}(-1, 1, -1, 1, -1, 1),
\end{aligned} \tag{13}$$

where

$$\boldsymbol{\Phi} = \begin{bmatrix} \boldsymbol{\Phi}_{11} & \boldsymbol{\Phi}_{12} & \boldsymbol{\Phi}_{13} \\ \boldsymbol{\Phi}_{21} & \boldsymbol{\Phi}_{22} & \boldsymbol{\Phi}_{23} \\ \boldsymbol{\Phi}_{31} & \boldsymbol{\Phi}_{32} & \boldsymbol{\Phi}_{33} \end{bmatrix},\ \boldsymbol{\Phi}_{ij} = c_i c_j \begin{bmatrix} -1 & -1 \\ 1 & 1 \end{bmatrix},\ (i,j = 1,2,3).$$

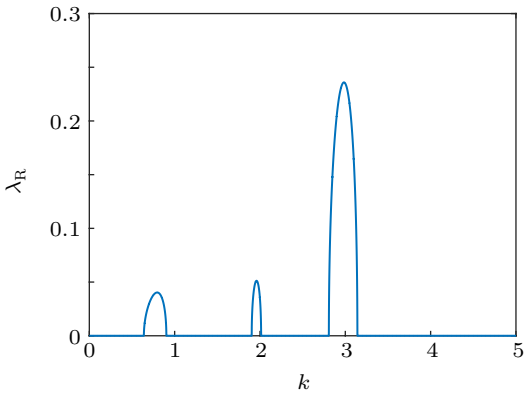


Fig. 1. The relation between the maximum real part λ_R and modulation frequency k, the parameters are $c_1 = c_2 = 0.5$, $c_3 = 0.1$, $a_1 = \pi$, $a_2 = 0$, $a_3 = \pi/3$.

According to the knowledge of linear differential equations with constant coefficients, we can obtain the fundamental matrix solution

$$\widetilde{U} = [\mathrm{e}^{\lambda_1 t}\boldsymbol{V}_1, \mathrm{e}^{\lambda_2 x}\boldsymbol{V}_2, \ldots, \mathrm{e}^{\lambda_6 x}\boldsymbol{V}_6], \tag{14}$$

where λ_i are the eigenvalues satisfying the characteristic equation $\det(\lambda\mathbb{I} - \boldsymbol{H}) = 0$, and $\boldsymbol{V}_i$ are corresponding eigenvectors. Then we can study the eigenvalues to judge the linear stability. The characteristic equation $\det(\lambda\mathbb{I} - \boldsymbol{H}) = 0$ can reduce into

$$\sum_{i=1}^{3} \frac{c_i^2}{(a_i - \mathrm{i}\lambda')^2 - \frac{k^2}{4}} = 1, \tag{15}$$

where $\lambda' = \lambda/k$. Since the characteristic equation about λ is a hexagonal polynomial, the discriminant is very complex. We ignore to give it. Thus the judgement of MI can be claimed: Once the characteristic root has positive real part, the corresponding solutions must be MI. To visualize the process of MI, we plot Fig. 1 to exhibit the MI. In Fig. 1, with the choice of parameters, the root of the polynomial has positive real part λ_R for some corresponding k values, so the general nonzero background possesses modulational instability. However, although the general nonzero background is modulationally unstable, not all components of the general nonzero background are modulationally unstable. Modulation stable region still exists here. Then we discuss Eqs. (15) and (20) (in the next section), which represent the modulational stability of the general nonzero background and the existence of dark soliton, respectively. The form of two equations is very similar. On the other hand, it is well known that the modulational stability analysis is an important factor for the generation of Akhmediev breather and rogue waves[33] cannot be used to explain the existence of dark solitons. However, we still conjecture that

there is a certain relationship between modulational stability of background and the existence of dark soliton, which would be disclosed in the future work.

3. Dark solitons on the general nonzero background

In this section, we mainly intend to study the behavior of dark solitons on the general nonzero background and find some new phenomena to further enrich the nonlinear system.

3.1. The single-dark-soliton solutions for TCNLS equations

The single dark soliton solutions on the plane wave background can be derived directly by the Darboux transformation.[21,34] After the original single-soliton solutions go through the $SU(3)$ transformation, the new one-dark-soliton solutions on the general nonzero background can be written as

$$q_{n1} = q_n - \sum_{m=1}^{3} A_{nm} c_m T_m (1+\tanh E) \mathrm{e}^{\mathrm{i}(a_m x - g_m t)}, \ (n=1,2,3), \tag{16}$$

where $E = -\lambda_{1\mathrm{I}}[x+(\lambda_{1\mathrm{R}}+h)t]$, $T_k = \frac{2\mathrm{i}\lambda_{\mathrm{I}}}{\lambda_1+h+a_m}$, $(m=1,2,3)$, λ_1 is a complex number $(\lambda_1 = \lambda_{1\mathrm{R}} + \mathrm{i}\lambda_{1\mathrm{I}})$, q_n are given by Eq. (3), and h is a parameter, which is connected with λ_1. Through the above expressions (16), we know the peak of dark soliton is along $x+(\lambda_{1\mathrm{R}}+h)t$, so we can obtain the velocity of dark soliton:

$$v = -(\lambda_{1\mathrm{R}} + h), \tag{17}$$

and the amplitudes of the dark soliton in the three-components are different from each other:

$$p_i \equiv \sum_{i=1}^{3} \frac{A_{ni}^2 c_i^2 \lambda_{1\mathrm{I}}^2}{(\lambda_{1\mathrm{R}}+h+a_i)^2 + \lambda_{1\mathrm{I}}^2}, \ (n=1,2,3). \tag{18}$$

In the literature,[21] the authors used the plane wave seed solution to solve the Lax pair equation. From Ref. [21], we can obtain the parameter matrix $\boldsymbol{U}_0$. Then we study the relationship between h and λ_1. Consider the characteristic matrix

$$\det(\lambda_1 \mathbb{I} - \boldsymbol{U}_0) = 0, \ \ \boldsymbol{U}_0 = \begin{bmatrix} h & -c_1 & -c_2 & -c_3 \\ c_1 & -h-a_1 & 0 & 0 \\ c_2 & 0 & -h-a_2 & 0 \\ c_3 & 0 & 0 & -h-a_3 \end{bmatrix}, \tag{19}$$

where λ_1 is the eigenvalues. By the mathematical calculation, we obtain the equation between h and λ_1 as follows:

$$\sum_{i=1}^{3} \frac{c_i^2}{|\lambda_1 + a_i + h|^2} = 1. \tag{20}$$

Then we have a conclusion on the condition of parameters. The dark solitons exist only if equation (20) possesses at least a pair of complex roots with respect to h. So we plot Fig. 2 to show the relationship between h and λ_1, which can be greatly helpful for us to select the parameter h. Similarly, we can judge the effective range of h by the selected parameters in the next research, which can ensure the existence of the dark solitons.

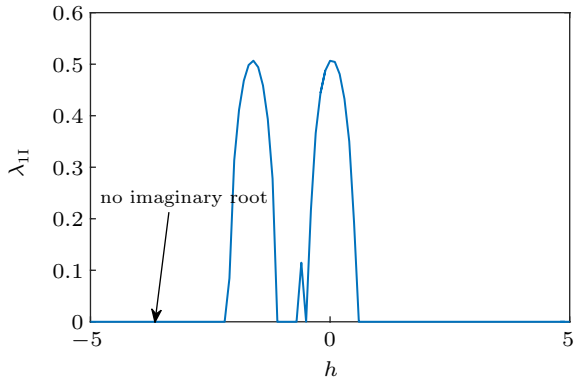


Fig. 2. The relationship between h and $\lambda_{1\mathrm{I}}$, the parameters are $c_1 = c_2 = 0.5$, $c_3 = 0.1$, $a_1 = \pi$, $a_2 = 0$, $a_3 = \pi/3$.

3.2. The multi-dark-soliton solutions for TCNLS equations

The multi-dark-soliton solutions on the plane wave background can also be derived by the Darboux transformation.[21,34] It has shown that the interaction among the dark solitons on plane wave background is elastic and dark solitons hold their shape and intensity or cause a slight oscillation about the phase, which will be a big effect in the quantum transmission.[35] With the number of the dark solitons increasing, the interaction among solitons will be more complex, so we just discuss the situation of two dark solitons. Comparing with the plane wave background, we study the phenomena on the general nonzero background. We can use the two-dark-soliton solutions to model the BECs and to simulate the collision on the general nonzero background. After the original two-dark-soliton solutions together with unitary transformation $SU(3)$, the new two-dark-soliton solutions can be written as

$$q_{n2} = \sum_{l=1}^{3} A_{nl} c_l \frac{|\boldsymbol{N}^{[l]}|}{|\boldsymbol{N}|} \mathrm{e}^{\mathrm{i}(a_l x - g_l t)}, \ \ (n=1,2,3), \tag{21}$$

where both $\boldsymbol{N}$ and $\boldsymbol{N}^{[l]}$ $(l=1,2,3)$ are 2×2 matrices and they can be written as

$$\begin{aligned} \boldsymbol{N}_{ij} &= \frac{2[\mathrm{e}^{\mathrm{i}(Y_j - Y_i^*)} + \eta_{ij}]}{(h_j+\lambda_j) - (h_i+\lambda_i)}, \\ \boldsymbol{N}_{ij}^{[l]} &= \boldsymbol{N}_{ij} - 2\frac{\mathrm{e}^{\mathrm{i}(Y_j - Y_i^*)}}{h_j+\lambda_j+a_l}, \ \ (i,j=1,2), \end{aligned} \tag{22}$$

with the symbol * representing the conjugation, and

$$Y_i = \lambda_i x + (\lambda_i h_i + \frac{1}{2}\lambda_i^2 - \frac{1}{2}h_i^2)t, \quad \eta_{ji} = \begin{cases} 0, & j \neq i, \\ \mathrm{e}^{\alpha_i}, & j = i, \end{cases} \tag{23}$$

where α_i $(i=1,2)$ equal to zero. The relations between the parameter h_i and λ_i are as follows:

$$\sum_{m=1}^{3}\frac{c_m^2}{|\lambda_i+a_m+h_i|^2}=1,\quad (i=1,2). \tag{24}$$

The situation is the same as the single-dark-soliton solution, we can also find the effective value of parameters h_i to ensure the existence of two dark solitons.

3.3. The dynamics for the dark solitons on the general nonzero background

Compared with the previous backgrounds (plane wave background, stripe phase background, etc.), the general nonzero background has more colorful dynamics than the previous ones. Under this background, we can add the dark solitons and observe many fascinating dynamic behaviors which have never been reported before. In the following, we mainly study and discuss case Ⅲ (the parameters $(a_i,\ i=1,2,3)$ are unequal with each other) in Section 2. According to different phenomena, we can roughly classify them into four categories, which are named as cases i, ii, iii, and iv, respectively. Comparing the expression about the amplitude of background and soliton and considering the randomness of matrix $\boldsymbol{A}$, we can only discuss the values of $c_1^2+c_2^2+c_3^2$ and $c_1c_2+c_2c_3+c_1c_3$. To make dark solitons visible in the background, the amplitude of dark soliton must be much higher than the amplitude of background, i.e., $(c_1^2+c_2^2+c_3^2)\gg(c_1c_2+c_2c_3+c_1c_3)$, or $c_1\gg c_2,c_3$. For the aesthetic effect of background, we must opt appropriate parameters (a_1,a_2,a_3) to prevent background waves from becoming too dense or too sparse. In other words, the spatial period of background $(\frac{2\pi}{a_i-a_j},\ (i,j=1,2,3))$ can not be too large or too small. We give the specific classification in the following.

Case i Assume the parameters a_i $(i=1,2,3)$ are arranged in ascending order, i.e. $a_1<a_2<a_3$, and the parameters c_i $(i=1,2,3)$ satisfy $c_1\gg c_2,c_3$. Especially, we choose the parameters $(c_1=5,\ c_2=1,\ c_3=1,\ a_1=-0.1,\ a_2=0.1,\ a_3=0.8)$ to plot Fig. 3, which look like a mountain range. The upper row is for single dark soliton, and the single dark solitons cross the peaks. The lower row is for two dark solitons, where it is shown that the collision between two dark solitons is elastic, but the collisions cause a slight oscillation about the phase in their intersection, which is the same behavior as the two dark solitons on plane wave background.

Case ii Assume the parameters a_i $(i=1,2,3)$ are arranged in ascending order, i.e. $a_1<a_2<a_3$, and the parameters c_i $(i=1,2,3)$ satisfy $c_2\gg c_1,c_3$. Choosing the special parameters $(c_1=0.5,\ c_2=3,\ c_3=0.5,\ a_1=-0.3,\ a_2=0.3,\ a_3=1)$ to plot Fig. 4, we obtain the figures look like wave fringes. The upper row is for single dark soliton, these figures show that the dark soliton can propagate stably on general nonzero background. The lower row is for two dark solitons, the background wave fringes still do not affect the collision between two dark solitons.

Case iii Assume the parameters a_i $(i=1,2,3)$ are arranged in ascending order, i.e. $a_1<a_2<a_3$, and the parameters c_i $(i=1,2,3)$ satisfy $c_3\gg c_1,c_2$. Choosing the parameters $(c_1=0.5,\ c_2=0.5,\ c_3=4,\ a_1=-0.2,\ a_2=0.2,\ a_3=1)$ to plot Figs. 5(a)–5(f). These figures appear to be different phenomena. Figures 5(a), 5(c), 5(d) and 5(f) look like a mountain range, while figures 5(b) and 5(e) look like wave fringes. It can also be demonstrated that the propagation of the dark soliton on the general nonzero background is stable and the interaction of two dark solitons is existent.

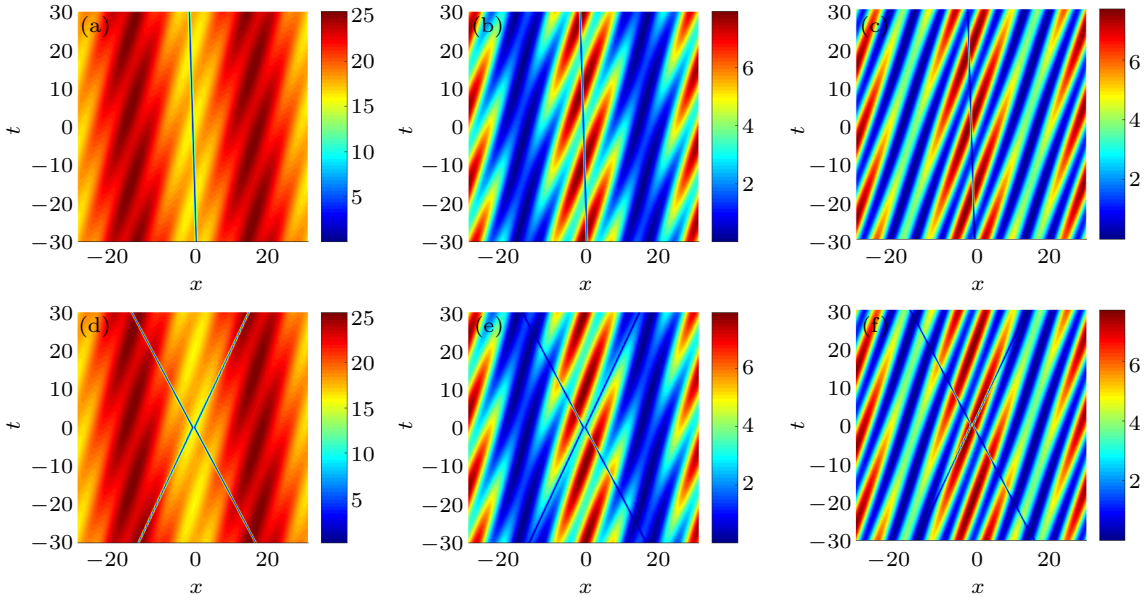


Fig. 3. Dark solitons on the general nonzero background. Here (a), (b), and (c) are the model square map of single dark soliton for q_{11}, q_{21}, and q_{31}, respectively; (d), (e), and (f) are the model square map of two dark solitons for q_{12}, q_{22}, and q_{32}, respectively. The parameters $c_1=5,\ c_2=1,\ c_3=1,\ a_1=-0.1,\ a_2=0.1,\ a_3=0.8$.

Case iv Assume the parameters a_i $(i = 1,2,3)$ are arranged in ascending order, i.e. $a_1 < a_2$, $a_3 \gg a_1$, and the parameters c_i $(i = 1,2,3)$ satisfy $(c_1^2 + c_2^2 + c_3^2) > (c_1c_2 + c_2c_3 + c_1c_3)$. We choose the parameters $(c_1 = 2,\ c_2 = 2,\ c_3 = 0.5,\ a_1 = -0.2,\ a_2 = 0.2,\ a_3 = 3)$ to plot Fig. 6. The upper row is for single dark soliton. The lower row is for two dark solitons. The period of variation along time t direction is greatly reduced, so the figures look more dense. On the whole, it is very similar to the stripe background,[31] which can be regard as infinitesimal t-period (case Ⅱ), and we can observe Fig. 6(a), where the behavior of dark soliton is not obvious, because the amplitude of dark soliton is not too much different from the amplitude of background, the dark soliton is suppressed by the background.

The above four figures all demonstrate that the dark soliton can propagate stably and continuously on the general nonzero background, the collision between two dark solitons is elastic. The stability of collision on the plane wave background has been already proved before, but on the general nonzero background is the first time, which not only further strengthens the theory of the invariance of solitons collision, but also promotes the further study of soliton stability. The four figures are the representational phenomena from general nonzero background. The other cases can be derived in a similar method.

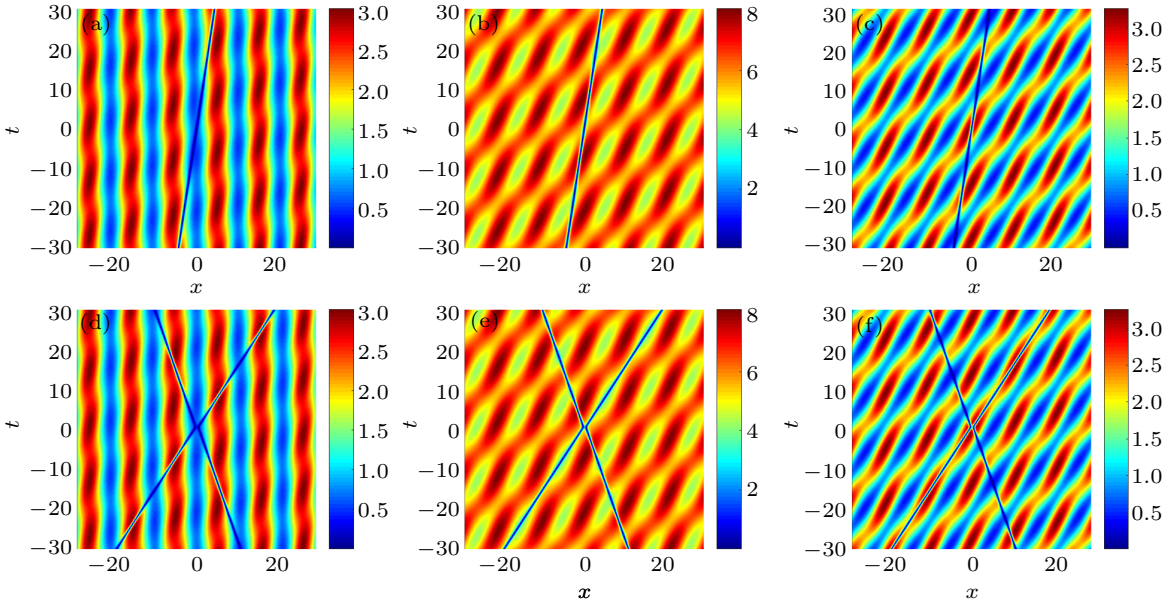


Fig. 4. Dark solitons on the general nonzero background. Here (a), (b), and (c) are the model square map of single dark soliton for q_{11}, q_{21}, and q_{31}, respectively; (d), (e), and (f) are the model square map of two dark solitons for q_{12}, q_{22}, and q_{32}, respectively. The parameters $c_1 = 0.5$, $c_2 = 3$, $c_3 = 0.5$, $a_1 = -0.3$, $a_2 = 0.3$, $a_3 = 1$.

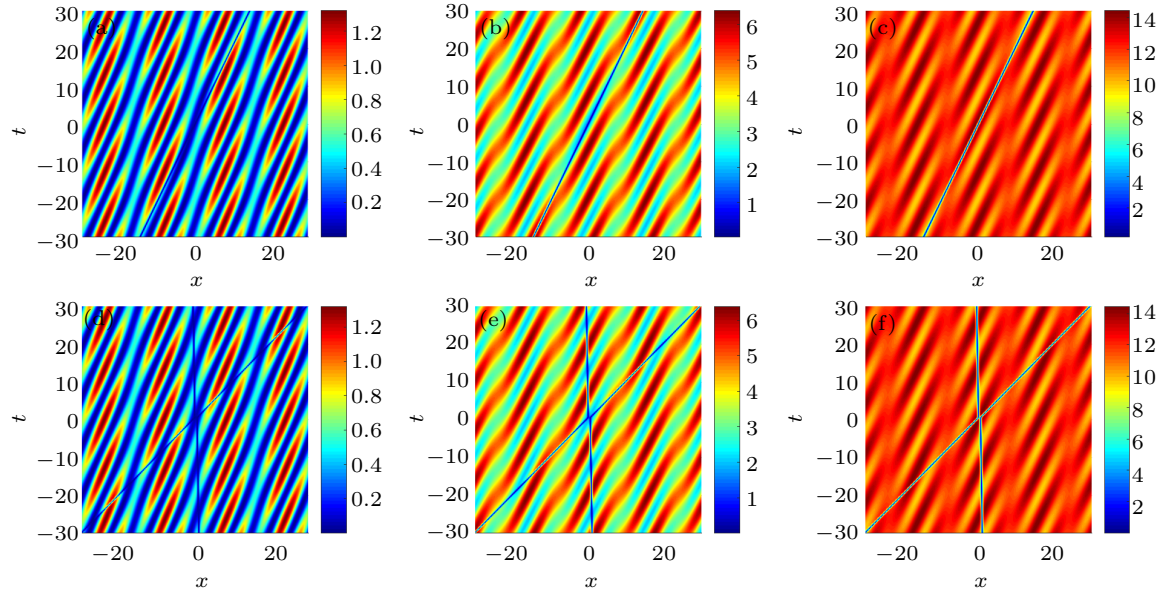


Fig. 5. Dark solitons on the general nonzero background. Here (a), (b), and (c) are the model square map of single dark soliton for q_{11}, q_{21}, and q_{31}, respectively; (d), (e), and (f) are the model square map of two dark solitons for q_{12}, q_{22}, and q_{32}, respectively. The parameters $c_1 = 0.5$, $c_2 = 0.5$, $c_3 = 4$, $a_1 = -0.2$, $a_2 = 0.2$, $a_3 = 1$.

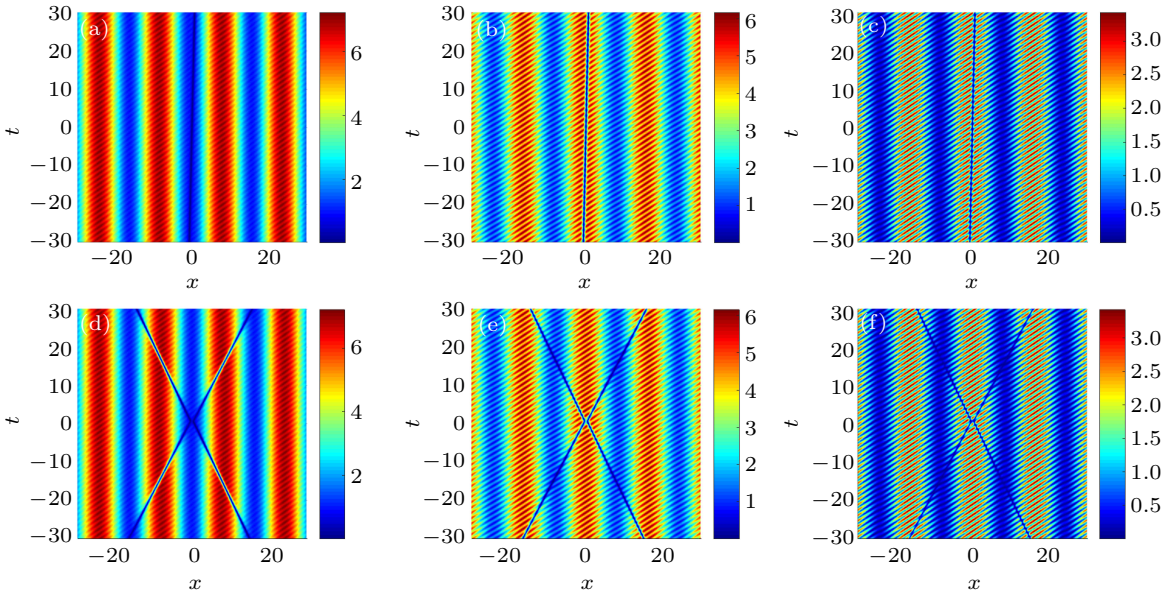


Fig. 6. Dark solitons on the general nonzero background. Here (a), (b), and (c) are the model square map of single dark soliton for q_{11}, q_{21}, and q_{31}, respectively; (d), (e), and (f) are the model square map of two dark solitons for q_{12}, q_{22}, and q_{32}, respectively. The parameters $c_1 = 2$, $c_2 = 2$, $c_3 = 0.5$, $a_1 = -0.2$, $a_2 = 0.2$, $a_3 = 3$.

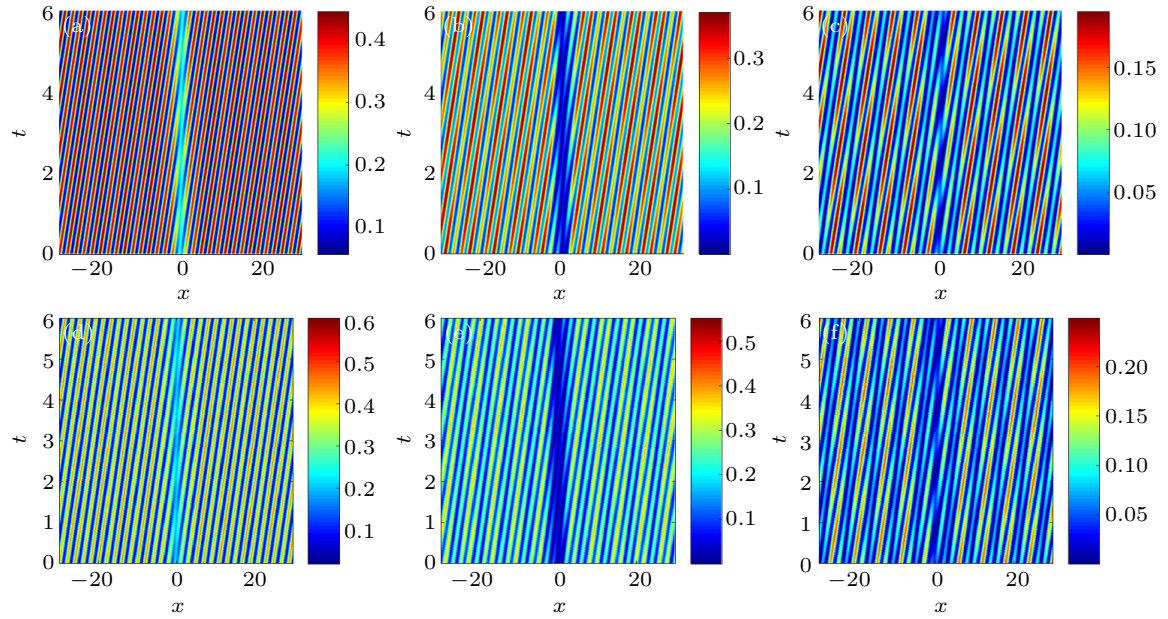


Fig. 7. Upper: the actual single-dark soliton on the general nonzero background. Here (a), (b), and (c) are the model square map for q_{11}, q_{21}, and q_{31}, respectively, which are the exact solutions, and the parameters are $c_1 = 0.5$, $c_2 = 0.5$, $c_3 = 0.1$, $a_1 = \pi$, $a_2 = 0$, $a_3 = \pi/3$. Lower: the numerical simulation for TCNLS equations under an initial condition. Here we use the single soliton solutions from exact solutions as the initial value; (d), (e) and (f) are the model square map for q_{11}, q_{21}, and q_{31}, respectively.

3.4. Numerical stability test

In the above subsection, we exhibit several interesting kinds of different dynamics of single dark soliton and two dark soliton solutions on the general nonzero background. For a physical system, the stability of solution is an important criterion to observability in experiments. Thus we use the numeric method to study the stability of these dark solitons. For convenience, we just test one dark soliton on the fluctuated background.

In Fig. 1, when k is small, the roots of characteristic equation are not all positive real part, where we know that the general nonzero background solutions may be stable under this condition. In the following, we choose the same parameters as Fig. 1 to discuss the numerical stability of dark soliton solutions. Then we test the numerical stability of one dark soliton on the general nonzero background. Firstly, we use the same parameters as before and set the $h = 0$ to plot Figs. 7(a)–7(c), which are the exact solutions. Here the choice of the parameters belongs to case iv. Departing from the initial condition about the single-dark soliton at time $t = 0$ with a small white noise, and combining the Fast Fourier Transform with fourth-order Runge–Kutta method and carrying out numeri-

cal evolution, we can obtain the numerical solutions showing in Figs. 7(d)–7(f). The variation of errors E between the exact solution and the numerical solution with respect to time t (Fig. 8) shows that the dark soliton on the fluctuated background is stable against the white noise, which further verifies the observability in experiments.

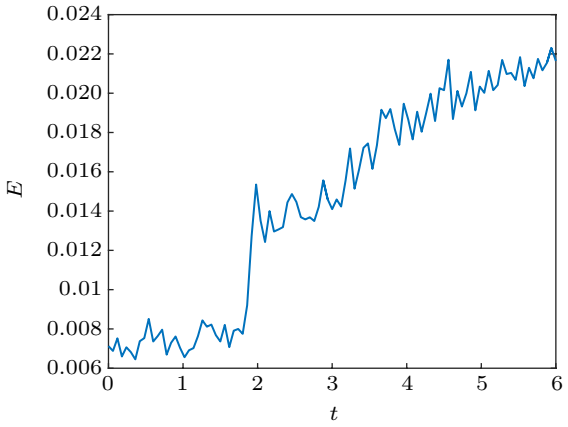


Fig. 8. The error E between the exact solutions and the numerical solutions (Fig. 7) about time t.

4. Conclusion

In summary, we have studied the dynamics of a single dark soliton and two dark solitons on the general nonzero background for the TCNLS equations. The phenomena we obtain in this paper possess much more complicated dynamics. Then we analyze the MI of the fluctuated background, where we find that the background may be modulational stability in certain parameters. The dynamics of the dark solitons and the collision of two dark solitons on the general nonzero background are shown by computer graphics. Furthermore, we use the numerical method and add the white noise to test the numerical stability of dark solitons, which shows that they are robust against the white noise. We believe that the dark soliton on fluctuated background can be observed in the physical experiments in the near future.

References

[1] Gerdjikov V S 2009 *AIP Conf. Proc.* **1186** 15
[2] Zhang Y, Nie X J and Zha Q L 2014 *Phys. Lett. A* **378** 191
[3] Kurihara S 1981 *Phys. B+C* **107** 413
[4] Du Z, Tian B, Chai H P and Yuan Y Q 2019 *Commun. Nonlinear Sci. Numer. Simul.* **67** 49
[5] Zhao L C, Yang Z Y and Yang W L 2019 *Chin. Phys. B* **28** 010501
[6] Liu Y K, Li B 2017 *Chin. Phys. Lett.* **34** 010202
[7] Wang X B and Han B 2019 *Europhys. Lett.* **126** 15001
[8] Zhao L C, Ling L M, Qi J W, Yang Z Y and Yang W L 2017 *Commun. Nonlinear Sci. Numer. Simul.* **49** 39
[9] Burger S, Bongs K, Dettmer S, Ertmer W, Sengstock K, Sanpera A, Shlyapnikov G V and Lewenstein M 1999 *Phys. Rev. Lett.* **83** 5198
[10] Wang Z H, Cherkasskii M, Kalinikos B A, Carr L D and Wu M Z 2014 *New J. Phys.* **16** 053048
[11] Guo B L and Wang Y F 2016 *Wave Motion* **67** 47
[12] Li H, Wang D N and Cheng Y S 2009 *Chaos Solitons Fractals* **39** 1988
[13] Liu X X, Pu H, Xiong B, Liu W M and Gong J B 2009 *Phys. Rev. A* **79** 013423
[14] Ling L M and Zhao L C 2015 *Phys. Rev. E* **92** 022924
[15] Qu C L, Pitaevskii L P and Stringari S 2016 *Phys. Rev. Lett.* **116** 160402
[16] Yu W T, Ekici M, Mirzazadeh M, Zhou Q, Liu W J 2018 *Optik* **165** 341
[17] Frantzeskakis D J 2010 *J. Phys. A: Math. Theor.* **43** 213001
[18] Ohta Y, Wang D S and Yang J K 2011 *Stud. Appl. Math.* **127** 345
[19] Mahalingam A and Porsezian K 2001 *Phys. Rev. E* **64** 046608
[20] Priya N V and Senthilvelan M 2016 *Commun. Nonlinear Sci. Numer. Simul.* **36** 366
[21] Ling L M, Zhao L C and Guo B L 2015 *Nonlinearity* **28** 3243
[22] Conforti M, Baronio F and Degasperis A 2011 *Physica D: Nonlinear Phenomena***240** 1362
[23] Li S Q 2012 *Third Global Congress on Intelligent Systems* (Wuhan, China 6–8 November 2012) p. 352
[24] Zhao X S, Li L and Xu Z Y 2009 *Phys. Rev. A* **79** 043827
[25] Gadzhimuradov T A, Abdullaev G O and Agalarov A M 2017 *Nonlinear Dyn.* **89** 2695
[26] Huang Q M 2019 *Appl. Math. Lett.* **93** 29
[27] Su J J and Gao Y T 2017 *Superlattices Microstruct.* **104** 498
[28] Lan Z Z, Gao B and Du M J 2018 *Chaos Solitons Fractals.* **111** 169
[29] Li L, Zhao X S and Xu Z Y 2008 *Phys. Rev. A* **78** 063833
[30] Shin H J 2005 *J. Phys. A: Math. Gen.* **38** 3307
[31] Lan Y, Zhao L C and Luo X W 2019 *Commun. Nonlinear Sci. Numer. Simul.* **70** 334
[32] Matveev V B 2007 *Philos. Trans.: Math. Phys. Eng. Sci.* **366** 837
[33] Zhao L C and Ling L M 2016 *J. Opt. Soc. Am. B* **33** 850
[34] Zhang H Q and Wang Y 2018 *Nonlinear Dyn.* **91** 1921
[35] Zhang H Q and Yuan S S 2017 *Commun. Nonlinear Sci. Numer. Simul.* **51** 124